Band structure of holes in p-type δ-doping quantum wells and superlattices

G. M. Sipahi, R. Enderlein, L. M. R. Scolfaro, and J. R. Leite
Instituto de Física da Universidade de São Paulo, Caixa Postal 66318, 05389-970 São Paulo, São Paulo, Brazil
(Received 25 September 1995; revised manuscript received 6 December 1995)

p-type δ-doping quantum wells and superlattices are semiconductor systems of considerable interest for basic research and device applications. In this paper, a method for calculating potentials and band structures of such systems is developed. The method relies on a plane-wave expansion of the multiband effective-mass equation, uses kinetic energy matrices of any size, and takes exchange correlation into account in a more rigorous way than this was done before. The method is used to calculate potential profiles, subband and miniband structures, as well as Fermi level positions for a series of p-type δ-doping quantum wells and superlattices. Exchange-correlation effects turn out to be rather large. Only if they are properly taken into account reasonable agreement with experimental photoluminescence data can be achieved. For comparison, potentials and energy levels are also calculated for electrons of n-type δ-doping systems. The potential wells for electrons are considerably deeper and wider, and exchange-correlation effects are less pronounced than for holes. The physical reasons for these differences and their implications on luminescence spectra from n- and p-type δ-doping structures are discussed.

I. INTRODUCTION

Semiconductors with δ-like layers of dopant atoms are challenging systems for basic research and device applications.[1] As compared with δ-doping structures of n-type,[1–22] those of p-type represent relatively new achievements.[23–31] Although p-type doping by means of Beryllium, during the molecular beam epitaxy growth of GaAs, has been widely used already, since the original work in Ref. 32, Beryllium δ doping in GaAs has been reported only recently.[23–27,29,30] It was clearly demonstrated in the work by Schubert *et al.*[24] Secondary-ion-mass spectroscopy and capacitance-voltage measurements allowed these authors to conclude that the spread of the doping layer was less than 2 nm. Relatively high sheet doping concentrations in the range of 10^{13} cm^{-2} were achieved so that hole confinement effects were likely to occur. Such effects have, in fact, been observed in photoluminescence (PL) spectra from Be $-\delta$-doped layers.[26,27,29,30] In order to enhance spectral features due to the confined holes, in Refs. 26,29, the δ-doped layers were placed between (Al,Ga)As barriers, providing better wave function overlap for the recombining electron-hole pairs in this way. PL signals from Be$-\delta$-doped layers in GaAs have been observed, however, also without (Al,Ga)As barriers.[27,29,30] The same observation has been reported for C$-\delta$-doped layers in GaAs.[28] This is in remarkable contrast to n-type δ-doping QW's, which never gave rise to detectable luminescence signals without confining the minority carriers (holes in this case) between barriers.

p-type δ-doping QW's and SL's have also been subjected to theoretical studies. Self-consistent band structure calculation for holes in such systems have been performed by various authors,[29,33,34] using the Luttinger-Kohn multiband effective-mass equation of the Γ_8 valence band complex.[35] This equation was solved self-consistently without[29] and with[33,34] exchange-correlation effects taken into account. The effective-mass equation was transformed into a matrix equation either with respect to a certain set of auxiliary functions, which had to be calculated numerically first,[29,33] or with respect to plane waves.[34] No further approximations on the Luttinger-Kohn Hamiltonian were made in Refs. 33 and 34, while axial symmetry perpendicular to the δ-doping plane was assumed in Ref. 29. From the above mentioned calculations, potential wells, subband energies, and Fermi level positions were obtained for single[29,33] and multiple[34] well structures. The calculated subband and Fermi level positions were compared with those derived from luminescence spectra. Rough agreement was stated in Ref. 29, and notable differences in Ref. 33. In Ref. 33, the importance of exchange-correlation effects was stressed in order to account for the relatively large light-to-heavy hole splittings observed experimentally.[26–29] In Ref. 34 it was pointed out that, for a more rigorous comparison between theory and experiment, the calculation of subband energies does not suffice, since the positions of luminescence peaks are also determined by the energy dependence of the radiative electron-hole recombination probability. The latter is governed by the overlap integral of electron and hole wave functions. This integral varies strongly with energy, since tunneling of electrons into hole wells (i.e., electron barriers) and/or of holes into hole barriers must take place to make the overlap nonzero.

Despite the already existing work, the hole problem in p-type δ-doping QW's and SL's needs further theoretical investigations. The opportunities and challenges of this problem have only partially been realized so far. We will mention only few of them. First, unlike QW's and SL's based on heterostructures, in p-type δ-doping QW's and SL's, only the potential operator of the multiband effective mass equation is spatially inhomogeneous, while the kinetic energy operator is constant in space, because of the homogeneous material composition. This means that the effective-mass equation applies at all points of the QW or SL, as opposed to heterostructure QW's or SL's, where it holds only within the homogeneous material layers, while the interfaces between them have to be bridged by boundary conditions. The latter are controversial among different authors and may introduce uncontrollable errors.[36] The effective mass theory of δ-doping QW's and SL's is free of such uncertainties. Moreover, the eigenvalue problem may be solved by means of the matrix method, without any restrictions on the set of basis

functions. In the case of heterostructure QW's and SL's, such restrictions result from the representation of the kinetic energy operator, which calls for material dependent basis functions. For δ-doping QW's and SL's, any reasonable set of basis functions may be used. Plane waves are particularly suited for two reasons: the kinetic energy operator is originally given with respect to them, and the Poisson equation transforms into a simple algebraic equation if written in the plane-wave representation.

Second, the hole potential of p-type δ-doping QW's and SL's is essentially codetermined by the hole gas itself, unlike to heterostructure QW's and SL's, where the gas introduces only small corrections to the potential, the main part of which arises from band discontinuities. The hole-hole interaction thus plays a key role in p-type δ-doping QW's and SL's. Although an analogous situation exists in n-type QW's and SL's, the two types of systems behave differently. Since typical experimental sheet concentrations are almost one order of magnitude higher in p-type δ-doping structures than in n-type structures, one could argue that exchange-correlation effects should be less important in p-type structures, as compared to n-type ones. This is true as long as one compares the exchange-correlation potential with the repelling Hartree potential only. The latter is, however, only part of the total one-particle potential without exchange correlation, the attracting potential due to the fixed sheet dopant charges has yet to be added. Owing to the strong localization of heavy holes, the two potential parts should compensate each other more completely in p-type than in n-type structures. Thus, in p-type structures, exchange-correlation effects are expected to play a particularly large role. This calls for a more sophisticated treatment of these effects, as compared to a procedure in which one takes the exchange-correlation potential of the Luttinger-Kohn hole gas as a diagonal matrix with the exchange-correlation potentials of heavy and light holes as diagonal elements.[33]

Third, δ-doping QW's and SL's have metallic character. In calculating their self-consistent Hartree potentials, the sum upon the occupied hole states has to be taken in each $\mathbf{k}$ point below the Fermi surface rather than in special points only as can be done in the case of the completely filled valence bands of semiconductors.[37] For the electrons of a n-type δ-doping well, isotropic and parabolic band dispersion may be assumed parallel to the layers which allows the $\mathbf{k}$ sum to be performed analytically. The isotropic approximation does, however, not apply to holes, in this case, the $\mathbf{k}$ sum has to be calculated numerically. As known from band structure calculations of bulk metals, this represents a rather time consuming but unavoidable procedure.

Fourth and last, unlike GaAs/(Ga,Al)As heterostructure QW's and SL's, in δ-doping QW's and SL's, only carriers of one type feel wells and are confined, while those of the other type feel barriers and are extended over the whole structure with the exception of the barrier regions from which particles having energies below the barrier are expelled. As already has been mentioned, the probabilities for optical transitions between such extended and confined electron and hole states are continuous and strongly varying functions of the energies of extended particles, unlike transitions between electron and hole states in GaAs/(Ga,Al)As heterostructure QW's and SL's, where no such energy dependence exists. In calculating luminescence and other optical spectra from δ-doping QW's and SL's, one needs, therefore, both electron and hole wave functions in numerical form. Calculating them from independent models for electrons and holes as it was done in Ref. 38 represents a possible but not an ideal solution. More appropriate would be their calculation by means of a model that applies to electrons and holes. This means the use of the Kane model for both types of carriers (as has been done in Ref. 39 for heterostructure SL's) instead of the Luttinger-Kohn model for holes and a one-band effective-mass equation for electrons. Thus, if luminescence spectra from δ-doping QW's and SL's are to be calculated, the Kane model should be used even in the case of GaAs being a material which is otherwise well described by the Luttinger-Kohn model. This calls for a simple solution procedure of the effective-mass equation in order to keep the numerical effort in reasonable limits. The matrix method with plane waves as a basis set, which has been used in Ref. 34, fulfills this demand.

The purpose of the present paper is to describe this method in greater detail and, by applying it, to calculate potential profiles and band structures for a series of p-type δ-doping QW's and SL's in the experimentally interesting ranges of doping concentrations and periods. The paper is organized as follows. In Sec. II, we present the method. The problem of the proper treatment of exchange-correlation effects for the two-component hole gas is approximately solved by deriving an exchange-correlation potential matrix with off-diagonal elements. In Sec. III, the potential profiles, subband and miniband dispersions in $\mathbf{k}$ space, as well as Fermi level positions, are calculated. The results are discussed in Secs. III and IV. In Sec. IV, a comparison with other theoretical findings and experimental luminescence spectra is made. Electron potentials and band structures of n-type δ-doping SL's with identical parameters are calculated and compared with the results for holes. Pronounced differences are found between the two types of carriers and explained in physical terms. Since we are not dealing with optical spectra of GaAs p-type δ-doping QW's and SL's in the present paper, and thus do not need hole and electron wave functions obtained from the same calculations, the Luttinger-Kohn model is used throughout. The method may be easily applied to other models including that by Kane. Calculations for luminescence spectra from p-type δ-doping QW's, using the Kane model, are in progress.

II. METHOD

A. Direct and reciprocal lattices

We consider a p-type δ-doped zinc blende type SL with the growth direction parallel to [001]. Assuming an even number N of Ga-As double layers per SL period, the Bravais lattice of the structure becomes tetragonal, and the primitive lattice vectors $\mathbf{A}_1, \mathbf{A}_2, \mathbf{A}_3$ of the SL may be chosen as

$$\mathbf{A}_1 = \frac{a}{2}(\mathbf{e}_x - \mathbf{e}_y), \quad \mathbf{A}_2 = \frac{a}{2}(\mathbf{e}_x + \mathbf{e}_y), \quad \mathbf{A}_3 = d\,\mathbf{e}_z, \tag{1}$$

where $\mathbf{e}_x, \mathbf{e}_y, \mathbf{e}_z$ denote unit vectors parallel to the cubic axes, a means the lattice constant of the zinc blende type crystal, and $d = 1/2\,Na$ the lattice constant of the SL in growth di-

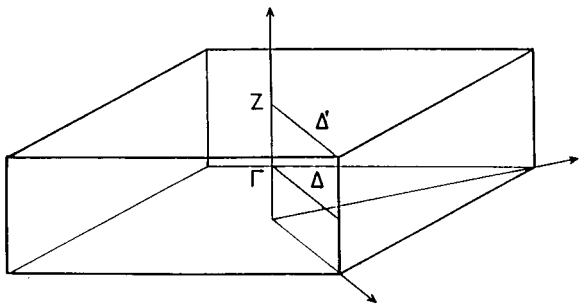

FIG. 1. First BZ of a δ-doping SL, as considered in this paper.

rection. Infinite extension of the SL is assumed in all three directions of space, and periodic boundary conditions are used in order to switch over to a finite periodicity region. The vectors spanning this region are $G_\parallel \mathbf{A}_1$, $G_\parallel \mathbf{A}_2$, and $G_z \mathbf{A}_3$, with $G_\parallel$ and G_z being large integers. One periodicity region contains $G_\parallel^2 G_z$ SL unit cells and $G_\parallel^2 G_z \times N$ zinc blende unit cells of volume $\Omega_0 = a^3/4$. The periodicity volume Ω thus amounts to $G_\parallel^2 G_z \times N \Omega_0 = G_\parallel^2 G_z \times d \times a^2/2$.

The primitive vectors $\mathbf{B}_1, \mathbf{B}_2, \mathbf{B}_3$ of the reciprocal SL are given by

$$\mathbf{B}_1 = \frac{2\pi}{a}(\mathbf{e}_x + \mathbf{e}_y), \quad \mathbf{B}_2 = \frac{2\pi}{a}(\mathbf{e}_x - \mathbf{e}_y), \quad \mathbf{B}_3 = \left(\frac{4\pi}{Na}\right)\mathbf{e}_z. \quad (2)$$

The corresponding first BZ of the SL is shown in Fig. 1. Due to the periodic boundary conditions, only $\mathbf{k}$ values of the form

$$\mathbf{k} = \frac{k_1}{G_\parallel}\mathbf{B}_1 + \frac{k_2}{G_\parallel}\mathbf{B}_2 + \frac{k_3}{G_z}\mathbf{B}_3 \quad (3)$$

are allowed with k_1, k_2, k_3 being integers.

B. Schrödinger equation

In one-electron approximation, the Hamiltonian H_0 of an electron of the undoped zinc blende type crystal is given by the sum of the kinetic energy and the lattice periodic one-electron potential, which here includes the spin orbit interaction. The p-type δ-doping of the SL gives rise to an additional space charge density $\rho(\mathbf{x})$ determined by the distribution $N_A^-(\mathbf{x})$ of ionized acceptors and $p(\mathbf{x})$ of holes. The acceptor atoms are assumed to be completely ionized, thus $N_A^-(\mathbf{x})$ equals the doping profile $N_A(\mathbf{x})$. The latter is taken to be homogeneous perpendicular to z (for a discussion of this approximation see Ref. 21), and a sum of Gaussians centered at the nominal doping layers $z = nd$ parallel to z. Thus, one has

$$N_A(\mathbf{x}) = N_s \sum_{n=-\infty}^{\infty} \frac{1}{\sqrt{2\pi}\sigma} e^{-(z-nd)^2/2\sigma^2}, \quad (4)$$

where N_s means the sheet doping concentration of acceptor layers, and σ^2 the variance of the Gaussian distribution. The square root of the variance, i.e., σ, represents the mean distance of a doping atom from the nominal doping plane. It should not be mixed with the spread of the doping profile, which rather is given by the full width Δz of the Gaussian at half maximum. For the latter, one has $\Delta z = 2\sqrt{2\ln 2}\sigma = 2.355\sigma$. From computational reasons, rectangular doping profiles are sometimes used instead of Gaussian ones. In order to compare with Gaussian profiles, the width of the rectangle has to be put 2.355σ rather than σ. In this work, Gaussian profiles are chosen, because these are the distributions which are expected to result from a δ source under the effect of diffusion.[1]

In order to align the Fermi level of the δ-doping region with the Fermi level in the bulk, a certain background concentration of hole traps is necessary. The amount of holes to be trapped depends on the width w of the space charge region where this alignment takes place. It decays inversely proportional to w. If w is allowed to become infinitely large, the background charge density necessary for Fermi level alignment goes to zero, and its effect in the δ-doping region becomes negligible. We will use this approximation in what follows. The total charge density $\rho(\mathbf{x})$ is then given by the expression

$$\rho(\mathbf{x}) = e[p(\mathbf{x}) - N_A(\mathbf{x})]. \quad (5)$$

It gives rise to an additional electrostatic potential $V_C(\mathbf{x})$, and an exchange-correlation potential $V_{\mathrm{XC}}(\mathbf{x})$. The former is determined by Poisson's equation,

$$\Delta V_C(\mathbf{x}) = -\frac{4\pi e^2}{\epsilon}\rho(\mathbf{x}), \quad (6)$$

with ϵ being the dielectric constant. The one-electron Hamiltonian H of the SL becomes

$$H = H_0 + V_C(\mathbf{x}) + V_{\mathrm{XC}}(\mathbf{x}). \quad (7)$$

The spinor-eigenstates of this Hamiltonian may be taken in Bloch form $(\mathbf{x}s|\nu\mathbf{k})$, with $\mathbf{k}$ being a wave vector of the first SL-BZ, s the spin coordinate, and ν the band number. The corresponding Schrödinger equation reads

$$H(\mathbf{x}s|\nu\mathbf{k}) = E_\nu(\mathbf{k})(\mathbf{x}s|\nu\mathbf{k}), \quad (8)$$

with $E_\nu(\mathbf{k})$ being the Bloch band energies. The hole distribution $p(\mathbf{x})$ may be expressed in terms of the spinor components $(\mathbf{x}s|\nu\mathbf{k})$ as follows:

$$p(\mathbf{x}) = \sum_s \sum_{\nu k \in \text{empty}} |(\mathbf{x}s|\nu\mathbf{k})|^2, \quad (9)$$

where the second sum is taken over unoccupied Bloch states $\nu\mathbf{k}$, i.e., states which lost their electrons to the acceptor atoms.

C. Effective mass equation

In order to solve the Schrödinger equation (8), we adopt the multiband effective-mass theory in the formulation by Luttinger and Kohn.[35] Accordingly, we chose an orthonormalized set of Bloch functions of the fourfold degenerate valence band of the unperturbed zinc blende type crystal at Γ, and denote them by $(\mathbf{x}s|m)$, $m = \frac{3}{2}, \frac{1}{2}, -\frac{1}{2}, -\frac{3}{2}$. With $\mathbf{k}$ being a vector of the first BZ of the zinc blende type crystal, the corresponding Luttinger-Kohn functions $(\mathbf{x}s|m\mathbf{k})$ read

$$(\mathbf{x}s|m\mathbf{k}) = \frac{1}{\sqrt{\Omega}} e^{i\mathbf{k}\cdot\mathbf{x}} (\mathbf{x}s|m). \tag{10}$$

They form an orthonormalized set of functions, which may be used in order to represent the eigenfunctions $(\mathbf{x}s|\nu\mathbf{k})$ of the SL. Due to the periodicity of the SL, only $\mathbf{k}$ vectors of the form $\mathbf{k}+K\mathbf{e}_z$ will contribute, where $\mathbf{k}$ means a vector of the first SL-BZ, and $K=(2\pi/d)l$ a vector of the reciprocal SL (l denotes an integer). The Luttinger-Kohn functions $(\mathbf{x}s|m\mathbf{k}+K\mathbf{e}_z)$ for such $\mathbf{k}$ vectors of the zinc blende bulk BZ will be abbreviated as $(\mathbf{x}s|m\mathbf{k}K)$. One has

$$(\mathbf{x}s|m\mathbf{k}K) = \frac{1}{\sqrt{\Omega}} e^{i(\mathbf{k}+K\mathbf{e}_z)\cdot\mathbf{x}} (\mathbf{x}s|m). \tag{11}$$

The expansion of the SL eigenfunctions $(\mathbf{x}s|\nu\mathbf{k})$, with respect to this set, reads

$$(\mathbf{x}s|\nu\mathbf{k}) = \sum_{mK} (m\mathbf{k}K|\nu\mathbf{k})(\mathbf{x}s|m\mathbf{k}K), \tag{12}$$

and the Schrödinger equation (8) takes the form

$$\sum_{m'K'} (m\mathbf{k}K|H_0+V_C+V_{\mathrm{XC}}|m'\mathbf{k}K')(m'\mathbf{k}K'|\nu\mathbf{k}) = E_\nu(\mathbf{k})(m\mathbf{k}K|\nu\mathbf{k}). \tag{13}$$

The matrix $(m\mathbf{k}K|H_0|m'\mathbf{k}K')$ of the unperturbed Hamiltonian H_0 is diagonal with respect to K,K', and its diagonal elements are given by the Luttinger-Kohn matrix of the Γ_8 valence band of diamond or zinc blende type crystals.[35] By arranging rows and columns in the sequence $\frac{3}{2},\frac{1}{2},-\frac{1}{2},-\frac{3}{2}$ from left to right and, respectively, up to down, this matrix becomes

$$(m\mathbf{k}K|H_0|m'\mathbf{k}K') = \delta_{KK'} \begin{pmatrix} Q & S & R & 0 \\ S^* & T & 0 & R \\ R^* & 0 & T & -S \\ 0 & R^* & -S^* & Q \end{pmatrix}, \tag{14}$$

with

$$Q = -(\gamma_1+\gamma_2)(k_x^2+k_y^2) + (2\gamma_2-\gamma_1)(k_z+K)^2, \tag{15}$$

$$T = -(\gamma_1-\gamma_2)(k_x^2+k_y^2) - (2\gamma_2+\gamma_1)(k_z+K)^2, \tag{16}$$

$$R = -\sqrt{3}[\gamma_2(k_x^2-k_y^2) - 2i\gamma_3 k_x k_y], \tag{17}$$

$$S = i2\sqrt{3}\gamma_3(k_x-ik_y)(k_z+K). \tag{18}$$

The part (14) of the total Hamiltonian matrix means the effective kinetic energy operator of the envelope function equation. The matrices of the two potentials $V_C(\mathbf{x})$ and $V_{\mathrm{XC}}(\mathbf{x})$ have to be treated separately.

Coulomb potential

Since the Coulomb potential $V_C(z)$ is a smooth function on the atomic length scale, its matrix elements between different Bloch states m may be neglected, while its diagonal elements may be replaced by the matrix elements between normalized plane waves,

$$(z|K) = \frac{1}{\sqrt{G_z d}} e^{iKz}. \tag{19}$$

One has

$$(m\mathbf{k}K|V_C|m'\mathbf{k}K') = \delta_{mm'}(K|V_C|K'). \tag{20}$$

For the $(K|V_C|K')$ matrix, the Fourier transformed Poisson's equation (6) yields

$$(K|V_C|K') = \frac{4\pi e^2}{\epsilon} \frac{1}{|K-K'|^2}[(K|N_A|K') - (K|p|K')]. \tag{21}$$

Due to the charge neutrality of the periodicity region, the diagonal elements of the total charge density vanish, i.e., one has

$$(K|N_A|K) - (K|p|K) = 0. \tag{22}$$

The matrix $(K|N_A|K')$ with $N_A(z)$ from (4) may be readily calculated. One gets

$$(K|N_A|K') = \left(\frac{N_s}{d}\right) A(K-K'), \tag{23}$$

$$A(K) = \int_{-\infty}^{\infty} dz\, \cos(Kz) \frac{e^{-z^2/2\sigma^2}}{\sqrt{2\pi}\sigma}, \tag{24}$$

The coefficient $A(K)$ may be expressed in terms of the error function of complex arguments. Here we will not use this function, but take the integral in (24) numerically.

The matrix $(K|p|K')$ is obtained as follows. First, we rewrite the probability distribution $|(\mathbf{x}s|\nu\mathbf{k})|^2$ of an electron by means of the expansion (12) for $(\mathbf{x}s|\nu\mathbf{k})$. We get

$$|(\mathbf{x}s|\nu\mathbf{k})|^2 = \sqrt{\Omega} \sum_{m'} \sum_{m} \sum_{K''K'''} (m\mathbf{k}K''|\nu\mathbf{k})(\nu\mathbf{k}|m'\mathbf{k}K''') \times (z|K''-K''')(m\mathbf{0}|\mathbf{x}s)(\mathbf{x}s|m'\mathbf{0}). \tag{25}$$

From this expression, we remove the spatial fluctuations on the atomic length scale by averaging it with respect to a bulk unit cell and summing upon the spin coordinate s. The average value $\Sigma_s\overline{|(\mathbf{x}s|\nu\mathbf{k})|^2}$ becomes diagonal with respect to m,m', and its diagonal elements are approximately given by

$$\sum_s \overline{|(\mathbf{x}s|\nu\mathbf{k})|^2} = \sqrt{\Omega} \sum_{m} \sum_{K''K'''} (m\mathbf{k}K''|\nu\mathbf{k})(\nu\mathbf{k}|m\mathbf{k}K''') \times (z|K''-K'''). \tag{26}$$

By using this expression, the average hole density $p(z)$ being a function of z only becomes

$$p(z) = \sqrt{\Omega} \sum_{\nu k \in \text{empty}} \sum_{m} \sum_{K''K'''} (m\mathbf{k}K''|\nu\mathbf{k})(\nu\mathbf{k}|m\mathbf{k}K''') \times (z|K''-K'''). \tag{27}$$

This results in the plane-wave representation matrix,

$$(K|p|K')=\frac{1}{\Omega}P(K-K'), \tag{28}$$

$$P(K)=\sum_{\nu k\in \text{empty}}\sum_{m}\sum_{K''}(m\mathbf{k}K''|\nu\mathbf{k})(\nu\mathbf{k}|m\mathbf{k}K''-K). \tag{29}$$

Inserting the two expressions (23) and (27) in (21) yields

$$(K|V_C|K')=\frac{4\pi e^2}{\epsilon}\frac{1}{|K-K'|^2}\left[\frac{N_s}{d}A(K-K')-\frac{1}{\Omega}P(K-K')\right]. \tag{30}$$

Exchange-correlation potential

Parametrized expressions for the exchange-correlation potential of spatially inhomogeneous electron gases have been proposed by various authors in terms of local densities (for a review see Ref. 40). These expressions cannot, however, be applied to the hole gas of the Γ_8 valence band edge of zinc blende type crystals without modifications, as has been realized in Refs. 33 and 41. We follow the spirit of Ref. 41 in order to derive an explicit expression for the Luttinger-Kohn representation matrix $(m\mathbf{k}|V_{\mathrm{XC}}|m'\mathbf{k})$ of the exchange-correlation potential V_{XC} of the hole gas under consideration. The derivation will be performed in three steps.

In a first step, the exchange-correlation potential matrix will be written down with respect to the eigenstates $|e_\mu\mathbf{k})$ of the Luttinger-Kohn Hamiltonian for heavy ($\mu=\pm\frac{3}{2}$) and light ($\mu=\pm\frac{1}{2}$) holes, although it is finally required with respect to the Luttinger-Kohn basis $|m\mathbf{k})$. This step is necessary, because we want to transfer the parametrized expressions for the exchange-correlation potential of electrons to the exchange-correlation potential of holes. In deriving the matrix $(e_\mu\mathbf{k}|V_{\mathrm{XC}}|e_{\mu'}\mathbf{k})$, we apply two approximations. The first one concerns the off-diagonal elements. These are small, because the hole density $p(z)$ and, therefore, also the exchange-correlation potential, are smooth functions of z on the atomic length scale. In effective mass theory, off-diagonal elements of smooth potentials are neglected. The second approximation concerns the diagonal elements $(e_\mu\mathbf{k}|V_{\mathrm{XC}}|e_\mu\mathbf{k})$. These represent the exchange-correlation potentials of holes. Unlike the electrons, the effective masses of holes depend on the direction of $\mathbf{k}$, if warping of the Γ_8 valence band energy surfaces is taken into account, as we will do. Replacing the isotropic free electron mass m_0 in the exchange-correlation potential expression for electrons by the anisotropic masses of heavy and light holes, one obtains exchange-correlation potentials $V_{\mathrm{XC}(3/2)}$ and $V_{\mathrm{XC}(1/2)}$ for holes that depend on the direction of $\mathbf{k}$. The thus determined matrix,

$$(e_\mu\mathbf{k}|V_{\mathrm{XC}}|e_{\mu'}\mathbf{k})=\begin{pmatrix} V_{\mathrm{XC}(3/2)} & 0 & 0 & O \\ 0 & V_{\mathrm{XC}(1/2)} & 0 & 0 \\ 0 & 0 & V_{\mathrm{XC}(1/2)} & 0 \\ 0 & 0 & 0 & V_{\mathrm{XC}(3/2)} \end{pmatrix}, \tag{31}$$

has to be transformed back to the Luttinger-Kohn basis $|m\mathbf{k})$, in which the hole exchange-correlation potential is finally required. The numerical effort of the described procedure is, however, quite high. We, thus, use an isotropic approximation, arguing as follows. First, we replace the anisotropic hole masses by the isotropic experimental values, which average over all $\mathbf{k}$ directions. In the case of GaAs, these values are $0.475m_0$ and $0.0875m_0$,[42] and their mean square deviations are $0.148m_0$ and $0.0292m_0$ for heavy and light holes, respectively. The experimental values mentioned above are not far from the values $0.377m_0$ and $0.090m_0$ calculated without warping, i.e., using $\gamma_2=\gamma_3$ (for GaAs, one has $\gamma_2=2.1, \gamma_3=2.9$ (Ref. 42)). We use these numbers as justification for the neglect of warping in the exchange-correlation potential of holes. This approximation does not mean, of course, that warping is neglected throughout in our calculations. It is still present in the effective kinetic energy matrix (14), where it has a much larger effect.

Without warping, the effective masses $m^*_{3/2}$ and $m^*_{1/2}$ of, respectively, heavy and light holes are given by the expressions

$$m^*_{3/2}=\frac{1}{\gamma_1-2\gamma_2}m_0, \tag{32}$$

$$m^*_{1/2}=\frac{1}{2\gamma_2+\gamma_1}m_0. \tag{33}$$

The densities $p_{3/2}$ and $p_{1/2}$ of the two hole gases follow, respectively, from the equations

$$p_{|m|}=\frac{1}{3\pi^2}\left(\frac{2m^*_{|m|}}{\hbar^2}\right)^{3/2}E_F^{3/2},\quad |m|=\frac{3}{2},\frac{1}{2}, \tag{34}$$

where E_F means the Fermi level of holes measured with respect to the valence band edge. From these equations, E_F may be eliminated by means of the total hole density

$$p=p_{3/2}+p_{1/2}. \tag{35}$$

Using the above approximations and definitions, we write down explicit expressions for the exchange-correlation potentials $V_{\mathrm{XC}(3/2)}$ and $V_{\mathrm{XC}(1/2)}$ of the heavy and light hole gases. The parametrized exchange-correlation potential V_{XC} for electrons will be taken in the form of Hedin and Lundqvist.[43] For a homogeneous electron gas of effective mass m^* and density n embedded in a material of static dielectric constant ϵ, their expression reads

$$V_{\mathrm{XC}}=-\frac{e^2}{2\epsilon a_B^*}\left(\frac{2}{\pi\alpha r_s}\right)-\frac{e^2}{2\epsilon a_B^*}\left(\frac{2}{\pi\alpha}\right)0.0368\ln\left(1+\frac{21}{r_s}\right), \tag{36}$$

with $a_B^*=\epsilon(m_0/m^*)a_B$ being the effective Bohr radius, $\alpha=(4/9\pi)^{1/3}$ a numerical constant, and $r_s^{-1}=[(4\pi/3)a_B^{*3}n]^{1/3}$ the screening radius. According to Ref. 43, the first term in expression (36), which scales with r_s^{-1}, arises from exchange, and the second term scaling with $\ln(1+21/r_s)$ from Coulomb correlation. In adapting the exchange-correlation potential (36) to the two-component hole gas under consideration, this interpretation becomes essential. While statistical correlation giving rise to the exchange term in equation (36) occurs either between heavy holes or between light holes, but not between heavy *and* light

holes, Coulomb correlation giving rise to the correlation term in (36) acts also between different kinds of holes. This means that in writing down expression (36) for a particular kind of holes, in the first term of expression (36), the electron density has to be replaced by the partial density of that kind of holes, while in the second term, the total hole density has to be inserted. In this way, one obtains

$$V_{\mathrm{XC}(3/2)}=-\frac{e^2}{2\epsilon a^*_{B(3/2)}}\left(\frac{2}{\pi\alpha r_{s(3/2)}}\right)-\frac{e^2}{2\epsilon a^*_{B(3/2)}}\left(\frac{2}{\pi\alpha}\right)0.0368\ln\left(1+\frac{21}{R_{s(3/2)}}\right), \tag{37}$$

$$V_{\mathrm{XC}(1/2)}=-\frac{e^2}{2\epsilon a^*_{B(1/2)}}\left(\frac{2}{\pi\alpha r_{s(1/2)}}\right)-\frac{e^2}{2\epsilon a^*_{B(1/2)}}\left(\frac{2}{\pi\alpha}\right)0.0368\ln\left(1+\frac{21}{R_{s(1/2)}}\right), \tag{38}$$

where

$$a^*_{B|m|}=\epsilon\left(\frac{m_0}{m^*_{|m|}}\right)a_B, \tag{39}$$

$$r^{-1}_{s|m|}=\frac{m^{*1/2}_{|m|}}{(m^{*3/2}_{3/2}+m^{*3/2}_{1/2})^{1/3}}\left(\frac{4\pi}{3}a^{*3}_{B|m|}p\right)^{1/3}, \tag{40}$$

$$R^{-1}_{s|m|}=\left(\frac{4\pi}{3}a^{*3}_{B|m|}p\right)^{1/3}, \tag{41}$$

with $|m|=\frac{3}{2},\frac{1}{2}$.

With the derivation of expressions (37) and (38), the exchange-correlation potential matrix (31) in the basis of hole eigenstates is completely known. In a second step, it has to be transformed into the basis of Luttinger-Kohn functions. How this transformation can be performed is shown in Appendix A. It results in

$$(m\mathbf{k}|V_{\mathrm{XC}}|m'\mathbf{k})=\begin{pmatrix} Q_{\mathrm{XC}} & S_{\mathrm{XC}} & R_{\mathrm{XC}} & 0\\ S^*_{\mathrm{XC}} & T_{\mathrm{XC}} & 0 & R_{\mathrm{XC}}\\ R^*_{\mathrm{XC}} & 0 & T_{\mathrm{XC}} & -S_{\mathrm{XC}}\\ 0 & R^*_{\mathrm{XC}} & -S^*_{\mathrm{XC}} & Q_{\mathrm{XC}} \end{pmatrix}, \tag{42}$$

with

$$Q_{\mathrm{XC}}=\frac{1}{4}[V_{\mathrm{XC}(3/2)}+3V_{\mathrm{XC}(1/2)}]\left(\frac{k_x^2+k_y^2}{k^2}\right)+V_{\mathrm{XC}(3/2)}\left(\frac{k_z^2}{k^2}\right), \tag{43}$$

$$T_{\mathrm{XC}}=\frac{1}{4}[3V_{\mathrm{XC}(3/2)}+V_{\mathrm{XC}(1/2)}]\left(\frac{k_x^2+k_y^2}{k^2}\right)+V_{\mathrm{XC}(1/2)}\left(\frac{k_z^2}{k^2}\right), \tag{44}$$

$$R_{\mathrm{XC}}=-\frac{\sqrt{3}}{4}[V_{\mathrm{XC}(3/2)}-V_{\mathrm{XC}(1/2)}]\left(\frac{k_x-ik_y}{k}\right)^2, \tag{45}$$

$$S_{\mathrm{XC}}=i\frac{\sqrt{3}}{2}[V_{\mathrm{XC}(3/2)}-V_{\mathrm{XC}(1/2)}]\left(\frac{(k_x-ik_y)k_z}{k^2}\right). \tag{46}$$

If the exchange-correlation potentials of heavy and light holes were identical, then the matrix (42) would take diagonal form with all diagonal elements being equal to the assumed common value of $V_{\mathrm{XC}(3/2)}$ and $V_{\mathrm{XC}(1/2)}$. In reality, $V_{\mathrm{XC}(3/2)}$ and $V_{\mathrm{XC}(1/2)}$ differ appreciably, mainly due to the different densities of the heavy and light hole gases. From this point of view, no justification exists to replace the exchange-correlation matrix (42) by its diagonal elements only.

The exchange-correlation potential matrix (42) applies to a spatially homogeneous Γ_8 valence band hole gas. As is commonly done, inhomogeneities will be taken into account by means of the local density approximation, i.e., by using expressions (37) and (38) for an inhomogeneous hole gas as well. This will be done in the third step. Owing to the z dependence of the external potential, the exchange-correlation potential matrix (42) becomes also z dependent. Its $|m\mathbf{k}K)$ representation becomes nondiagonal with respect to K. This means that $(m\mathbf{k}|V_{\mathrm{XC}}|m'\mathbf{k})$ has to be replaced by $(m\mathbf{k}K|V_{\mathrm{XC}}|m'\mathbf{k}K')$, as well as Q_{XC}, T_{XC}, R_{XC}, S_{XC} by, respectively, $(K|Q_{\mathrm{XC}}|K')$, $(K|T_{\mathrm{XC}}|K')$, $(K|R_{\mathrm{XC}}|K')$, $(K|S_{\mathrm{XC}}|K')$. The latter matrices have to be calculated numerically from the z-dependent expressions of $Q_{\mathrm{XC}}(z)$, $T_{\mathrm{XC}}(z)$, $R_{\mathrm{XC}}(z)$, $S_{\mathrm{XC}}(z)$, which follow from equations (43) to (46) if there the z-dependent expressions $V_{\mathrm{XC}(3/2)}(z)$ and $V_{\mathrm{XC}(1/2)}(z)$ are inserted. The latter are obtained from expressions (37), (38) by using the z-dependent hole concentration according to equations (27), (34), and (35). One gets

$$(m\mathbf{k}K|V_{\mathrm{XC}}|m'\mathbf{k}K')=\begin{pmatrix} (K|Q_{\mathrm{XC}}|K') & (K|S_{\mathrm{XC}}|K') & (K|R_{\mathrm{XC}}|K') & 0\\ (K|S_{\mathrm{XC}}|K')^* & (K|T_{\mathrm{XC}}|K') & 0 & (K|R_{\mathrm{XC}}|K')\\ (K|R_{\mathrm{XC}}|K')^* & 0 & (K|T_{\mathrm{XC}}|K') & -(K|S_{\mathrm{XC}}|K')\\ 0 & (K|R_{\mathrm{XC}}|K')^* & -(K|S_{\mathrm{XC}}|K)^* & (K|Q_{\mathrm{XC}}|K). \end{pmatrix}, \tag{47}$$

with

$$(K|Q_{\mathrm{XC}}|K')=\frac{1}{4}[(K|V_{\mathrm{XC}(3/2)}|K')+3(K|V_{\mathrm{XC}(1/2)}|K')]\times\left(\frac{k_x^2+k_y^2}{k^2}\right)+(K|V_{\mathrm{XC}(3/2)}|K')\left(\frac{k_z^2}{k^2}\right), \quad (48)$$

$$(K|T_{\mathrm{XC}}|K')=\frac{1}{4}[3(K|V_{\mathrm{XC}(3/2)}|K')+(K|V_{\mathrm{XC}(1/2)}|K')]\times\left(\frac{k_x^2+k_y^2}{k^2}\right)+(K|V_{\mathrm{XC}(1/2)}|K')\left(\frac{k_z^2}{k^2}\right), \quad (49)$$

$$(K|R_{\mathrm{XC}}|K')=-\frac{\sqrt{3}}{4}[(K|V_{\mathrm{XC}(3/2)}|K')-(K|V_{\mathrm{XC}(1/2)}|K')]\times\left(\frac{k_x-ik_y}{k}\right)^2, \quad (50)$$

$$(K|S_{\mathrm{XC}}|K')=i\frac{\sqrt{3}}{2}[(K|V_{\mathrm{XC}(3/2)}|K')-(K|V_{\mathrm{XC}(1/2)}|K')]\times\left(\frac{(k_x-ik_y)k_z}{k^2}\right). \quad (51)$$

With the determination of the exchange-correlation potential matrix (47) of the inhomogeneous hole gas, the last step in setting up the Luttinger-Kohn effective mass equation (13) in plane-wave representation has been accomplished. The matrices of the three operators in this equation being the kinetic energy operator H_0, the Coulomb potential V_C, and the exchange-correlation potential V_{XC}, have different structures. That of H_0 is nondiagonal with respect to the angular momentum quantum numbers m, but diagonal with respect to the SL wave vectors K. For the matrix of V_C it holds exactly the opposite, it is diagonal with respect to m, but nondiagonal with respect to K, and for the matrix of V_{XC}, one has nondiagonal elements with respect to m and K. The eigenvalues and eigenvectors of the total matrix have to be calculated in a self-consistent way by using the eigenvector dependence of the Coulomb and exchange-correlation potentials specified before. The energy zero point is fixed at the barrier energy of the Coulomb potential throughout the calculations.

D. Convergency test

In order to check the convergency of the plane-wave expansion, we treat an isolated undoped square well. Due to the abrupt changes of the potential in this case, convergency is more critical than in the δ-doping case with its continuously varying potential. Thus, the square well test suffices. For the Luttinger parameters of GaAs, we take the following values:[42] $\gamma_1=6.85$, $\gamma_2=2.1$, $\gamma_3=2.9$. The hole subband structure of the square well is calculated with different numbers of plane waves. While pronounced changes are observed between 21 and 41 plane waves, the results for 41 plane waves do not alter considerably if one proceeds to 61 and 101. The anticrossing behavior of the subbands known from the calculations for heterostructure quantum wells[44] shows clearly up in the hole band structures calculated with 41 plane waves or more.

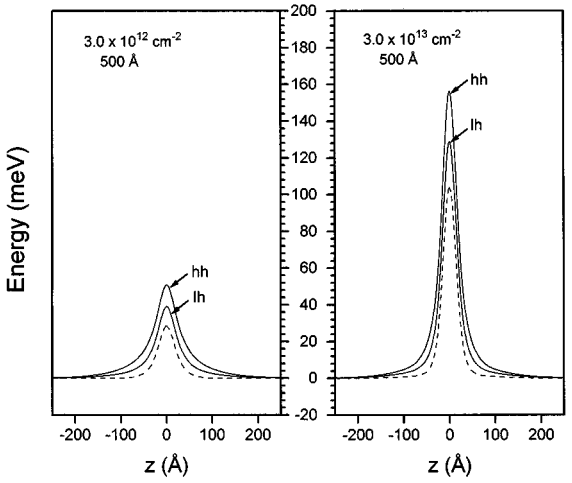

FIG. 2. Hole potentials for p-type δ-doping SL's of period $d=500$ Å; acceptor sheet concentrations 3×10^{12} cm^{-2} (left), and 3×10^{13} cm^{-2}; $\sigma=10$ Å. Dashed curves show the Coulomb potential, full curves give the total potential, including exchange correlation. The energy zero has been fixed at the Coulomb barrier potential for holes.

III. POTENTIALS AND BAND STRUCTURES OF p-TYPE δ-DOPING QW'S AND SL'S

We calculate hole potentials and band structures for p-type δ-doping QW's and SL's with different acceptor sheet concentrations and periods, covering the ranges of experimental interest. Accordingly, we adopt three different doping concentrations, being 3×10^{12} cm^{-2}, 8×10^{12} cm^{-2}, and 3×10^{13} cm^{-2}. For each concentration, the SL period is taken to be 500 Å in order to cover quasi-isolated QW's, and 200 Å in order to consider typical SL's. Altering the doping spread Δz will cause changes of the results. These will be investigated separately at the end of this section. Here, Δz is set 23.55 Å in all cases corresponding to $\sigma=10$ Å.

A. Potentials

In Fig. 2, potentials are shown for the lowest and the highest of the three doping concentrations mentioned above. Only potentials for the 500 Å SL's are depicted, because those for the 200 Å SL's differ only slightly. The dashed lines in Fig. 2 mean the Coulomb potential without exchange-correlation interaction, and the solid lines the total potential including this interaction. Two curves, at least, are necessary, in order to display the total potential because the exchange-correlation part of it is represented by a matrix $(m\mathbf{k}|V_{\mathrm{XC}}|m'\mathbf{k})$. For holes with quasi-wave-vectors $\mathbf{k}$ parallel to the z axis, the off-diagonal elements of this matrix disappear, and the diagonal elements become the exchange-correlation potentials of heavy and light holes. These are the exchange-correlation parts entering the total potential curves in Fig. 2. Curves marked with hh are the total potentials seen by heavy holes moving in z direction, and curves marked

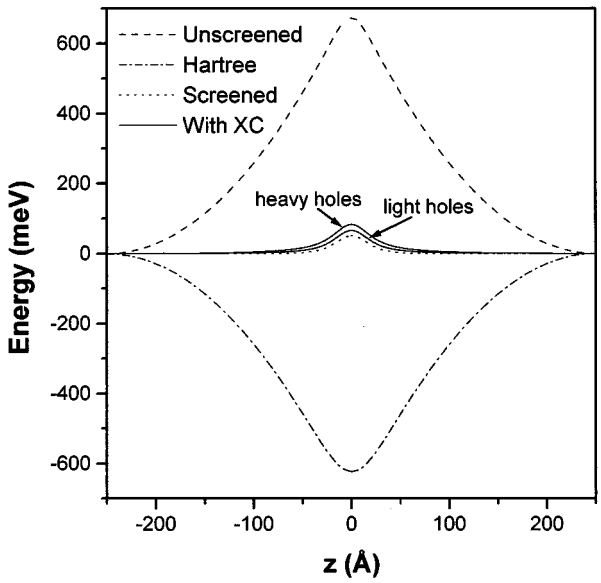

FIG. 3. Partial and total potentials for holes in a p-type δ-doping SL of period 500 Å and acceptor sheet concentration 8×10^{12} cm^{-2}. The unscreened potential is due to the negatively charged acceptor sheet, embedded in a spatially homogeneous hole gas in order to neutralize the total charge. The Hartree potential arises from the self-consistently calculated hole distribution embedded in a spatially homogeneous negative charge distribution, again for neutralizing the total charge. The screened potential means the total Coulomb potential seen by a hole. It represents the sum of the two former potentials. Shown are also the total potentials for heavy and light holes including exchange correlation.

with lh are the potentials seen by light holes moving in this direction. The heavy hole potentials are always deeper than the light hole potentials, first, because the exchange-correlation potential is attracting and monotonously increasing with density and, second, because the densities of heavy holes are always larger than those of light holes. Altogether, exchange-correlation effects are relatively large in the p-type δ-doping SL's under consideration. Similar conclusions have been drawn in Refs. 33,45. In our case, the relative contribution of exchange correlation to the total heavy hole potential ranges between 30% for higher doping concentrations and about 40% for lower. Such large relative contributions will not arise, of course, if the exchange-correlation potential is compared with the Hartree potential of holes only, without the unscreened Coulomb potential of the negatively charged acceptor sheet (see Fig. 3). The latter forms a deep well, which is almost completely screened out by the Hartree potential of holes. With respect to the Hartree potential, exchange correlation contributes only about 5% for heavy holes and 3% for light holes. The total well depths increase with rising doping concentrations. The depths of the heavy hole wells of the 500 Å SL's are, respectively, 48 meV, 85 meV, and 148 meV for the three doping concentrations mentioned above. For the 200 Å SL's, they take somewhat smaller values, due to the lower hole concentrations and consequently, smaller exchange-correlation potentials at the well centers. Generally, the hole wells considered here are less deep than the electron wells in n-type

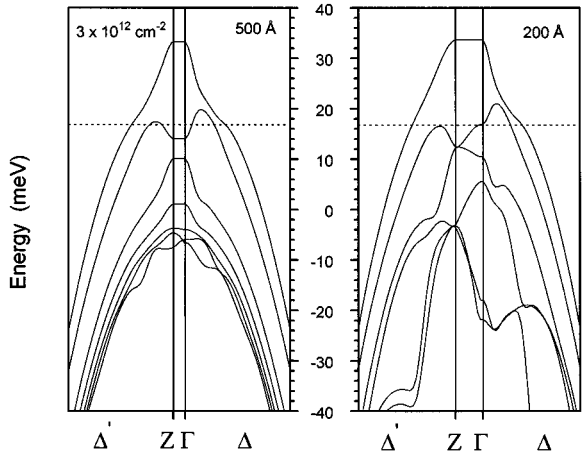

FIG. 4. Band structures (solid lines) and Fermi levels (dashed lines) for p-type δ-doping SL's of periods $d=500$ Å (left part) and $d=200$ Å (right part). Acceptor sheet concentration equal to 3×10^{12} cm^{-2}, $\sigma=10$ Å. Horizontal scale adjusted to the Γ-Z distance π/d. Energy zero as in Fig. 2.

δ-doping SL's at the same sheet doping concentration.[21] In Sec. IV, we will discuss this difference in greater detail.

B. Band structures

In Figs. 4–6, the band structures of the SL's are depicted. Each figure corresponds to a certain sheet doping concentration. In each figure the 500 Å SL is shown on the left hand side, and the 200 Å SL on the right hand side. Shown are the miniband dispersions perpendicular to the SL layers between the center of the first SL-BZ at Γ and its boundary at Z, as well as the subband dispersion along the Δ and Δ' lines parallel to the SL layers (see Fig. 1). The scales for wave vectors perpendicular and parallel are the same in each figure. They are determined by the Γ-Z distance, which amounts to π/d. For the 500 Å SL of doping concentration

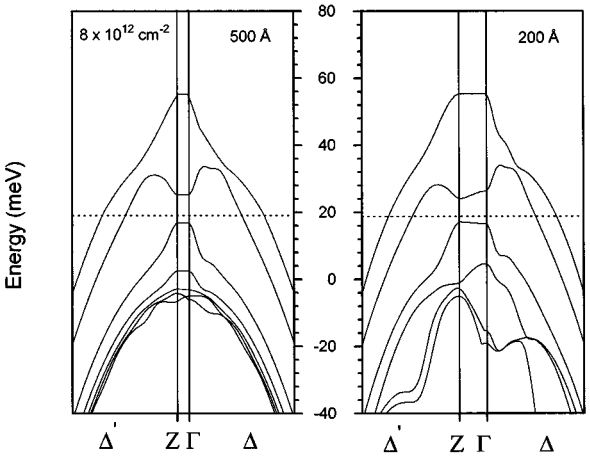

FIG. 5. Band structures (solid lines) and Fermi levels (dashed lines) for a p-type δ-doping SL of periods $d=500$ Å (left part) and $d=200$ Å (right part). Acceptor sheet concentration equal to 8×10^{12} cm^{-2}, $\sigma=10$ Å. Horizontal scale adjusted to the Γ-Z distance π/d. Energy zero as in Fig. 2.

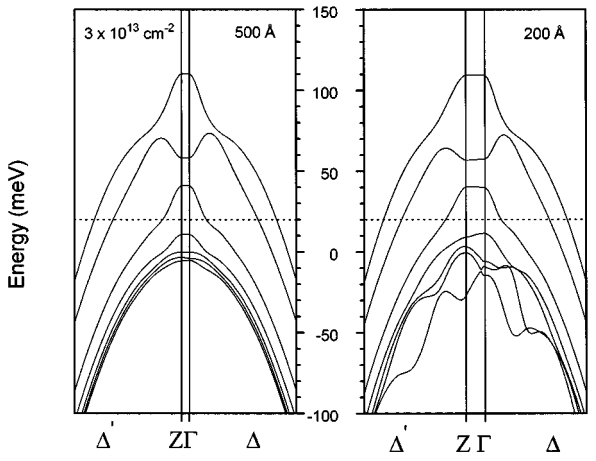

FIG. 6. Band structures (solid lines) and Fermi levels (dashed lines) for a p-type δ-doping SL of period $d=500$ Å (left part) and $d=200$ Å (right part). Acceptor sheet concentration equal to 3×10^{13} cm^{-2}, $\sigma=10$ Å. Horizontal scale adjusted to the Γ-Z distance π/d. Energy zero as in Fig. 2.

3×10^{12} cm^{-2} (Fig. 4), a dispersionless hh1 miniband at 33 meV below the common heavy and light hole barrier is followed by a dispersionless lh1 miniband at 14 meV. The hh2 and hh3 minibands are still below the barrier, while all higher minibands are above. The latter show considerable miniband dispersion. The subbands arising from hh and lh minibands for nonzero wave vector components $\mathbf{k}_\parallel$ parallel to the layers show strong anticrossing behavior, similar to heterostructure QW's (see, e.g., Ref. 44). Almost all holes are hosted by the hh1 subband, with only little occupation of the lh1 subband.

For the 200 Å SL of the same doping concentration 3×10^{12} cm^{-2} (see Fig. 4), strong miniband dispersion occurs already from the lh1 band on. The hh1 miniband is dispersionless, and occurs at the same energy as the hh1 miniband of the 500 Å SL. Again the hh1 subband is hosting almost all holes.

Increasing the sheet doping concentration deepens the wells and shifts the minibands up with respect to the well bottom. First, we consider the moderate doping case of 8×10^{12} cm^{-2} (Fig. 5). For both the 500 Å and the 200 Å SL, two hh minibands and two lh minibands occur below the barrier. The dispersionless hh1 minibands are 55 meV above the barrier for both SL's. Again, the dispersion of the corresponding subbands with respect to $\mathbf{k}_\parallel$ exhibits strong anticrossing behavior. The Fermi level lies in the second, i.e., the lh1 subband.

At the highest doping concentration 3×10^{13} cm^{-2} shown in Fig. 6, the minibands follow in the sequence hh1, lh1, hh2, hh3, lh2 for both the 500 and 200 Å SL's. The first three are almost dispersionless and occur at approximately the same energy in the two SL's being, respectively, 110 meV, 60 meV, and 40 meV. Deviations start from the hh2 miniband, which is dispersionless in the wider SL and shows dispersion in the narrower one. The nonparabolicity of the subband dispersion is clearly dominated by an anticrossing behavior. The Fermi level has moved up to the third subband in both SL's.

The doping spread $\Delta z=2.355\sigma$ has been fixed so far at 23.55 Å. In experiment, Δz may considerably differ from this value. Thus, we have calculated energy levels and Fermi energies as a function of Δz for the three 500 Å SL's considered above. The results are shown in Fig. 7. For a given doping concentration, the two hole wells become shallower and the Fermi level moves up if Δz increases, as is expected. The shifts of the hole levels with increasing Δz are the net result of two competing effects being the lowering of the well bottom, which moves the levels down, and the decrease of the confinement, which shifts the levels up. As can be seen from Fig. 7, the first effect dominates for the lowest heavy

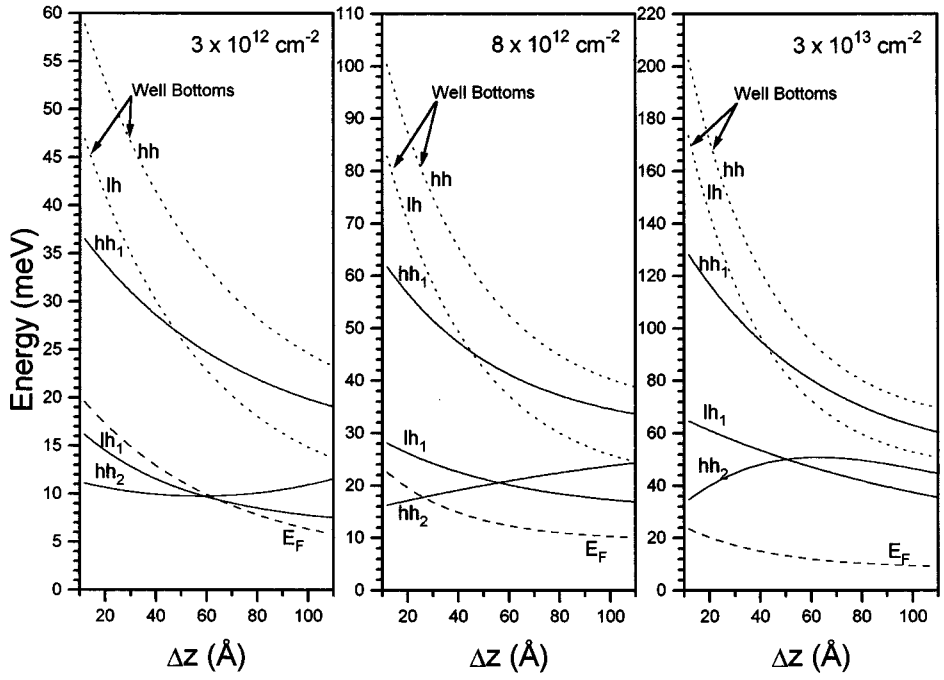

FIG. 7. Well bottoms (dotted lines), hole levels (solid lines), and Fermi energies (dashed lines), for p-type δ-doping 500 Å SL's, plotted against the doping spread Δz. Energy zero, as in Fig. 2. The three different doping concentrations 3×10^{12} cm^{-2}, 8×10^{12} cm^{-2}, and 3×10^{13} cm^{-2} are shown in different parts of the figure.

and light hole levels hh1 and lh1, and the second effect for the excited heavy hole level hh2. Due to this, the ordering of the hh2 level above the lh1 level at small Δz is reversed at large Δz. The Fermi level for the two SL's with lower doping concentrations which, at small Δz, lies above the hh1 and lh1 subband edges but below the hh2 edge, enters the hh2 subband at large Δz. Altogether, the above results indicate that the electronic structures of p-type δ-doping QW's are very sensitive to variations of the doping profile. Similar results have been found in previous calculations[29,33] (for a comparison with n-type δ-doping QW's see Sec. IV).

IV. DISCUSSION

A. Comparison with previous calculations

Isolated QW's with moderate doping concentration (8×10^{12} cm^{-2}) and small doping spread ($\approx$20 Å) have also been treated in Refs. 29,33, using methods and approximations (see Sec. I) differing from the present ones. The well depth of 135 meV from Ref. 33 is considerably larger than our value of 85 meV, while the depth of 90 meV obtained in Ref. 29 is close to our result. However, comparing the value obtained here with that from Ref. 29, one has to keep in mind that exchange correlation has not been taken into account in Ref. 29. If this would have been done, the well depth in Ref. 29 would also have been larger than ours. Generally, the approximations in Refs. 29,33 seem to result in an underestimation of the subband densities of states at low energies. As a consequence of this, hole states with higher energies are filled. These are less effective in screening out the negative acceptor sheet charge distribution, thus the potential well becomes deeper. In fact, the Fermi level lies in the second subband in Ref. 29, as in our calculations but by 10 meV higher, while in Ref. 33 it has even moved up into the third subband.

B. Comparison with experimental PL spectra

Experimental data on hole states in δ-doping wells may be obtained from PL spectra. Such spectra have been measured on isolated δ-doping QW's in Refs. 26–30. The spectra exhibit peaks, which may be attributed to radiative transitions between extended electron states and hole states confined to the δ-doping wells. Two peaks are resolved in most of the spectra, corresponding to transitions into the lowest heavy hole state hh1 and the lowest light hole state lh1. In comparing calculated transition energies with experimental peak positions, one has to be aware that no one-to-one correspondence can be expected, because these positions are also determined by the energy dependence of the overlap integral between electron and hole envelope functions.[38] Nevertheless, a rough comparison between theoretical level separations or level doping shifts and experimental peak separations or peak doping shifts should be possible. In order to be able to derive doping shifts of transition energies from hole level shifts, the hole levels have to be referred to the bottom of the conduction band. This is automatically done in our calculations: as the energy zero point has been fixed at the barrier of the Coulomb potential, the conduction band bottom occurs always at the gap energy E_g on our energy scale.

TABLE I. Experimental PL peak positions $P_{\rm hh1}$ and $P_{\rm lh1}$. Samples with no data for the doping spread Δz are indicated by "n.d."

N_A (10^{13} cm^{-2})	Δz (Å)	$P_{\rm hh1}$ (eV)	$P_{\rm lh1}$ (eV)	Ref.
0.8	n.d.	1.460	1.496	26
0.4	n.d.	1.485	1.493	27
1.8	n.d.	1.460	1.480	27
3.6	n.d.	1.430	1.460	27
0.3	65	1.480	1.494	29
0.8	72	1.460	1.480	29
3.0	125	1.450	1.466	29

Experimental values for the positions $P_{\rm hh1}$ and $P_{\rm lh1}$ of PL peaks arising from transitions to hh1 and lh1 states are summarized in Table I for various δ-doping samples. In all cases, *isolated* δ-doping layers have been measured. For a given doping concentration, the spacing $P_{\rm hh1}$-$P_{\rm lh1}$ between the two lowest PL peaks may be compared with the calculated subband level spacings $E_{\rm hh1}$-$E_{\rm lh1}$ at the subband bottom $\mathbf{k}_\parallel=0$. Such a comparison is shown in Table II. The experimental spacings from Ref. 29 compare well with the theoretical spacings calculated for the experimental doping spreads. For the samples measured in Refs. 26,27 no doping spreads are known, so that no definite statements on agreement or disagreement between theory and experiment can be made. One can, however, fit theoretical and experimental spacings to estimate the doping spread Δz. The results are given in parentheses in Table II.

In the experimental spectra,[27,29] the PL peaks shift to lower energies if the sheet doping concentration N_A is increased. This behavior is reproduced by the calculations: Although hole levels move down with respect to the well bottom if N_A increases, the bottom itself moves up resulting in a net up shift of the hole levels, and a down shift of the transition energy. The experimental down shifts $\Delta P_{\rm hh1}$ of the

TABLE II. Comparison of calculated energy level spacings and doping shifts with experimental PL data. For doping spreads Δz shown in parentheses, no experimental values were available; the given values were obtained by fitting level spacings $E_{\rm hh1}$-$E_{\rm lh1}$ and PL peak spacings $P_{\rm hh1}$-$P_{\rm lh1}$ (which then are identical by definition). If no experimental spread values existed, the level shifts $\Delta E_{\rm hh1}$ with increasing doping concentration have been calculated by means of the fitted values Δz. $\Delta P_{\rm hh1}$ denotes the experimental shift of the $P_{\rm hh1}$ peak with doping. All doping shifts are referred to the lowest concentration shown for the corresponding reference.

N_A (10^{13} cm^{-2})	Δz (Å)	$E_{\rm hh1}$-$E_{\rm lh1}$ (meV)	$P_{\rm hh1}$-$P_{\rm lh1}$ (meV)	$\Delta E_{\rm hh1}$ (meV)	$\Delta P_{\rm hh1}$ (meV)	Ref.
0.3	(5)	36	36	0	0	26
0.4	(110)	8	8	0	0	27
1.8	(110)	20	20	-22	-25	27
3.6	(90)	30	30	-50	-55	27
0.3	65	15	14	0	0	29
0.8	72	20	20	-16	-20	29
3.0	125	24	20	-25	-30	29

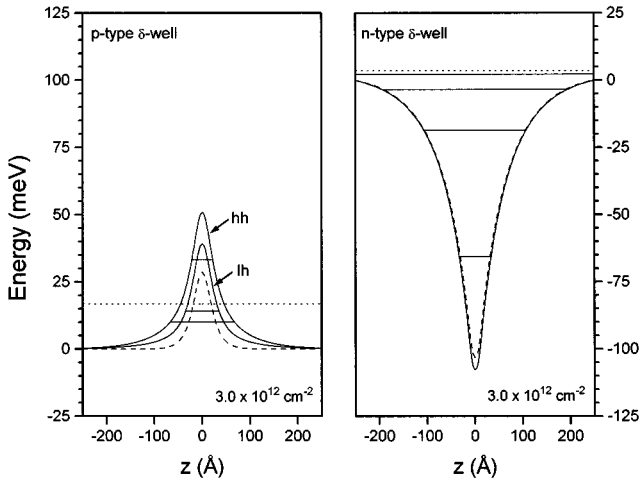

FIG. 8. Left hand part: Potential profiles and miniband levels (solid lines) of holes for a p-type δ-doping SL of period $d=500$ Å. The Coulomb potential (dashed line) and Fermi level (dotted line) are also shown. Acceptor sheet concentration equal to 3×10^{12} cm^{-2}, $\sigma=10$ Å. Right hand part: The same quantities as on the left hand side, but for electrons of an n-type δ-doping SL of the same doping concentration and period.

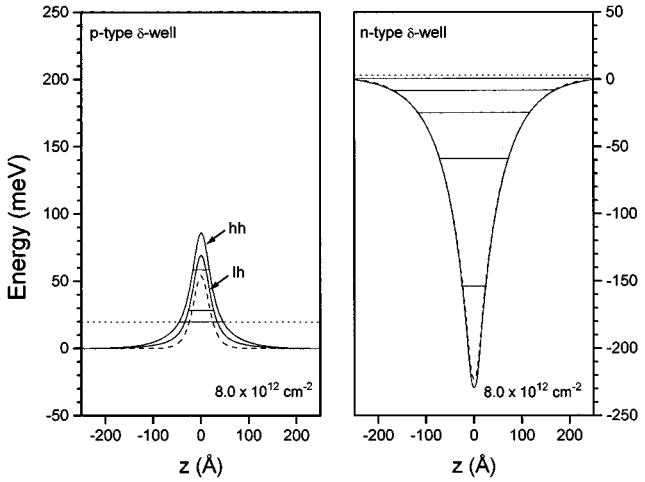

FIG. 9. Left hand part: Potential profiles and miniband levels (solid lines) of holes for a p-type δ-doping SL of period $d=500$ Å. The Coulomb potential (dashed line) and Fermi level (dotted line) are also shown. Acceptor sheet concentration equal to 8×10^{12} cm^{-2}, $\sigma=10$ Å. Right hand part: The same quantities as on the left hand side, but for electrons of an n-type δ-doping SL of the same doping concentration and period.

P_{hh1} peak are shown in Table II, together with the theoretical shifts ΔE_{hh1} calculated with Δz values from the same table. All shifts are referred to the lowest doping concentration reported in the respective reference. The comparison between ΔE_{hh1} and ΔP_{hh1} in Table II shows that reasonable agreement between theory and experiment can be stated also with respect to the doping shifts of PL peaks. The somewhat larger experimental shifts could be due to the doping induced band gap shrinkage, which has not been taken into account in our calculations.

C. Comparison between p- and n-type δ-doping wells

Deeper insight into the hole structure of p-type δ-doping wells can be obtained by a comparison with n-type δ-doping wells of the same or slightly lower sheet doping concentrations and periods. We will concentrate on the 500 Å SL. In the right hand parts of Figs. 8–10, the electron potentials as well as the miniband and Fermi levels are shown for the three sheet doping concentrations 3×10^{12} cm^{-2}, 8×10^{12} cm^{-2}, 1.5×10^{13} cm^{-2}, and a σ value of 10 Å. As before, solid curves are used for the total potentials including exchange correlation, and dashed curves for the potentials without exchange correlation. One notices that the wells for electrons are considerably wider and deeper than those for holes shown in the left hand parts of Figs. 8–10. This may be easily understood in terms of localization and screening. Due to their larger effective-mass, heavy hole states are stronger localized at the δ sheet than light holes and electrons. From the same reason, heavy holes form the ground state of the p-type δ-doping well, which implies that most of the holes are heavy. Because of their stronger localization, they screen the sheet charge distribution more effectively than the weaker localized light holes and electrons (if the localization at the sheet was perfect, the screening would be complete).

Another difference between n- and p-type δ-doping structures, concerning the dependence of their electronic structures on the doping spread Δz, may be understood by means of similar arguments. As has been demonstrated in Sec. III, the barrier heights and level positions of p-type δ-doping QW's are very sensitive to variations of their doping profiles.

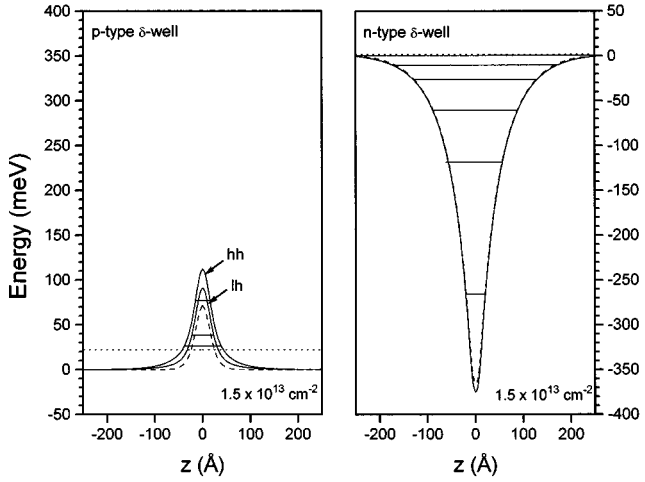

FIG. 10. Left hand part: Potential profiles and miniband levels (solid lines) of holes for a p-type δ-doping SL of period $d=500$ Å. The Coulomb potential (dashed line) and Fermi level (dotted line) are also shown. Acceptor sheet concentration equal to 1.5×10^{13} cm^{-2}, $\sigma=10$ Å. Right hand part: The same quantities as on the left hand side, but for electrons of an n-type δ-doping SL of the same doping concentration and period.

This contrasts with n-type δ-doping QW's, where this sensitivity has been found to be much less (see, e.g., Ref. 20). The above discussion provides a simple explanation also for this difference: As the heavy holes dominate in p-type δ-doping QW's, and the heavy holes are stronger localized in the vicinity of the doping sheet than the electrons of n-type δ-doping QW's, variations of the doping profile are felt much stronger by the holes than by the electrons.

Differences between electron and hole δ-doping structures exist also with respect to the role of exchange-correlation effects. From Figs. 8–10 one can see that exchange-correlation effects are stronger in the case of heavy holes than in that of electrons (and light holes). Two reasons are responsible for this. First, the higher density of the heavy hole gas, gives rise to a larger absolute value of the exchange-correlation potential. For heavy holes it amounts, respectively, to 23 meV, 32 meV, and 40 meV for the three concentrations, as opposed to 5 meV, 9 meV, and 12 meV for electrons. The second reason is more striking. It concerns the *relative* importance of the exchange-correlation potential, with respect to the Coulomb potential of fixed and mobile charges. The latter potential (shown by dashed curves in Figs. 8–10) is considerably smaller for holes than for electrons, because of the more complete screening by heavy holes. In this way, the relative contributions of exchange correlation to the total potentials in Figs. 8–10 amount to 44%, 30%, and 30% in the case of heavy holes, and only 6%, 4%, and 3% in the case of electrons.

Finally, the different depths of potential wells for $p-$ and n-type δ-doping structures should result in different intensities of luminescence light arising from the δ-doping regions. Since the larger depths and widths of n-type wells, as compared to p-type wells, make tunneling through electron wells more difficult than tunneling through hole wells, the overlap of electron and hole wave functions, and thus the luminescence intensities, should be much stronger for p-type QW's than for n-type QW's at the same sheet doping concentration. This could explain why experimentally n-type wells had to be placed between barriers in order to see luminescence, while p-type wells needed not.[38]

ACKNOWLEDGMENTS

The authors would like to thank CNPq, CAPES, FINEP, and FAPESP (Brazilian founding agencies) for partial financial support.

APPENDIX A

The hole eigenstates $|e_\mu \mathbf{k})$ follow from the Luttinger-Kohn basis $|m\mathbf{k})$ by means of an unitary transformation $U(\mathbf{k})$. One has

$$|e_\mu \mathbf{k}) = \sum_m U_{m\mu}(\mathbf{k}) |m\mathbf{k}). \tag{A1}$$

In order to obtain the matrix of the exchange-correlation operator V_{XC} in the Luttinger-Kohn basis $|m\mathbf{k})$ from that in the basis of eigenvectors, the unitary transformation (A1) has to be inverted. This results in

$$(m\mathbf{k}|V_{\mathrm{XC}}|m'\mathbf{k}) = \sum_\mu U_{m\mu}(\mathbf{k}) U^*_{m'\mu}(\mathbf{k}) (e_\mu \mathbf{k}|V_{\mathrm{XC}}|e_\mu \mathbf{k}). \tag{A2}$$

By using the explicit expression for $U_{m\mu}(\mathbf{k})$, the transformation (A2) may be readily carried out. This involves quite lengthy calculations. One may avoid them by exploiting the fact that, owing to the neglect of warping, the eigenvalues of the Luttinger-Kohn Hamiltonian are independent of the direction of $\mathbf{k}$. One has

$$(e_\mu \mathbf{k}|H_0|e_{\mu'}\mathbf{k}) = \begin{pmatrix} (2\gamma_2-\gamma_1) & 0 & 0 & 0 \\ 0 & -(2\gamma_2+\gamma_1) & 0 & 0 \\ 0 & 0 & -(2\gamma_2+\gamma_1) & 0 \\ 0 & 0 & 0 & (2\gamma_2-\gamma_1) \end{pmatrix} k^2. \tag{A3}$$

According to the definition of the unitary transformation $U(\mathbf{k})$, the matrix (A3) turns over into the matrix $(m\mathbf{k}|H_0|m'\mathbf{k})$ if the inverse transformation $U^+(\mathbf{k})$ is applied to it. This observation allows one to write down the matrix into which the exchange-correlation potential matrix (31) transforms by means of $U^+(\mathbf{k})$. One solely has to realize that the Hamiltonian matrix (A3) turns over into the matrix (31) if the replacements

$$\gamma_1 \to -\frac{1}{2k^2}[V_{\mathrm{XC}(3/2)} + V_{\mathrm{XC}(1/2)}], \tag{A4}$$

$$\gamma_2 \to \frac{1}{4k^2}[V_{\mathrm{XC}(3/2)} - V_{\mathrm{XC}(1/2)}] \tag{A5}$$

are made. Since the identity of the two matrices will hold also after their transformation with $U^+(\mathbf{k})$, the exchange-correlation energy matrix $(m\mathbf{k}|V_{\mathrm{XC}}|m'\mathbf{k})$ follows from the Hamiltonian matrix $(m\mathbf{k}|H_0|m'\mathbf{k})$ by replacing γ_1, γ_2 according to equations (A4) and (A5). In this way, one obtains expression (42) in the main text for $(m\mathbf{k}|V_{\mathrm{XC}}|m'\mathbf{k})$ with $Q_{\mathrm{XC}}, T_{\mathrm{XC}}, T_{\mathrm{XC}}, S_{\mathrm{XC}}$, from (43) to (46).

[1] E. F. Schubert, in *Epitaxial Microstructures*, edited by Arthur C. Gossard, Semiconductors and Semimetals Vol. 40 (Academic, New York, 1994), p. 1.
[2] K. Ploog, J. Cryst. Growth **81**, 304 (1987).
[3] E.F. Schubert, J. Vac. Sci. Technol. A **8**, 2980 (1990).
[4] H.P. Zeindl, T. Wegehaupt, I. Eisele, H. Oppolzer, H. Reisinger, G. Tempel, and F. Koch, Appl. Phys. Lett. **50**, 1164 (1987).
[5] N.L. Mattey, M.G. Dowsett, E.H.C. Parker, T.E. Whall, S. Taylor, and J.F. Zhang, Appl. Phys. Lett. **57**, 1648 (1990).
[6] A. Zrenner, F. Koch, and K. Ploog, Surf. Sci. **196**, 671 (1988).
[7] M. Santos, T. Sajoto, A. Zrenner, and M. Shayegan, Appl. Phys. Lett. **53**, 2504 (1988).
[8] M.H. Degani, J. Appl. Phys. **70**, 4362 (1991).
[9] S.M. Shibli, L.M.R. Scolfaro, J.R. Leite, C.A.C. Mendonça, F. Plentz, and E.A. Meneses, Appl. Phys. Lett. **60**, 2895 (1992).
[10] C.A.C. Mendonça, F. Plentz, J.B.B. Oliveira, E.A. Meneses, L.M.R. Scolfaro, D. Beliaev, S.M. Shibli, and J. R. Leite, Phys. Rev. B **48**, 12 316 (1993).
[11] L. Chico, F. García-Moliner, and V.R. Velasco, Phys. Rev. B **48**, 11 427 (1993).
[12] H. Jorke, H. Kibbel, F. Schäffler, A. Casel, H.-J. Herzog, and E. Kasper, Appl. Phys. Lett. **54**, 819 (1989).
[13] W. Kiunke, E. Hammerl, I. Eisele, D. Schulze, and G. Gobsch, J. Appl. Phys. **72**, 3602 (1992).
[14] H.-J. Gossmann and F.C. Unterwald, Phys. Rev. B **47**, 12 618 (1993).
[15] C.A.C. Mendonça, L.M.R. Scolfaro, J.B. Oliveira, F. Plentz, F. Mikovic, J.R. Leite, and E.A. Meneses, Superlatt. Microstruct. **12**, 257 (1992).
[16] W.-X. Ni, G.V. Hansson, J.-E. Sundgren, L. Hultman, L.R. Wallenberg, J.-Y. Yao, L.C. Markert, and J.E. Greene, Phys. Rev. B **46**, 7551 (1992).
[17] R. Enderlein, L.M.R. Scolfaro, J.M.V. Martins, J.R. Leite, F. Plentz, S.M. Shibli, and E.A. Meneses, Superlatt. Microstruct. **12**, 175 (1992).
[18] M.E. Lazzouni and L.J. Sham, Phys. Rev. B **48**, 8948 (1993).
[19] L.M.R. Scolfaro, A.T. Lino, E.K. Takahashi, and J.R. Leite, Int. J. Quantum. Chem. **S28**, 667 (1994).
[20] M.H. Degani, Phys. Rev. B **44**, 5580 (1991).
[21] L.M.R. Scolfaro, D. Beliaev, R. Enderlein, and J.R. Leite, Phys. Rev. B **50**, 8699 (1994).
[22] R. Enderlein, L.M.R. Scolfaro, and J.R. Leite, Phys. Rev. B **50**, 18 312 (1994).
[23] S.J. Pearton, F. Ren, C.R. Abernathy, W.S. Hobson, S.N.G. Chu, and J. Kovalchik, Appl. Phys. Lett. **55**, 1342 (1989).
[24] E.F. Schubert, J.M. Kuo, R.F. Kopf, H.S. Luftmann, C.L. Hopkins, and N.J. Sauer, J. Appl. Phys. **67**, 1969 (1990).
[25] A. Ourmazd, J. Cunningham, W. Jan, J.A. Rentschler, and W. Schröter, Appl. Phys. Lett. **56**, 854 (1990).
[26] J. Wagner, A. Ruiz, and K. Ploog, Phys. Rev B **43**, 12 134 (1991).
[27] A.M. Gilinsky, K.S. Zhuravlev, D.I. Lubyshev, V.P. Migal, V.V. Preobrashenskii, and B.R. Semiagin, Superlatt. Microstruct. **10**, 399 (1991).
[28] V.Ya. Aleshkin, A.V. Anshon, L.M. Batukova, E.V. Demidov, E.R. Demidova, B.N. Zvonkov, I.A. Karpovich, and I.G. Malkina, Fiz. Tekh. Poluprovodn. **26**, 1848 (1992) [Sov. Phys. Semicond. **26**, 1038 (1992)].
[29] D. Richards, J. Wagner, H. Schneider, G. Hensdorfer, and M. Maier, Phys. Rev. B **47**, 9629 (1993).
[30] M. El Allali, C.B. Sorensen, and E. Veje, J. Phys. (France) Colloq. IV **C5**, 299 (1993).
[31] Dan Ritter, R.A. Hamm, M.B. Panish, and M. Geva, Appl. Phys. Lett. **63**, 1543 (1993).
[32] M. Ilegems, J. Appl. Phys. **48**, 1278 (1977).
[33] F.A. Reboredo and C.R. Proetto, Phys. Rev. B **47**, 4655 (1993).
[34] G.M. Sipahi, R. Enderlein, L.M.R. Scolfaro, and J.R. Leite, *Proceedings of the 22nd International Conference on the Physics of Semiconductors*, edited by David J. Lockwood (World Scientific, Singapore, 1995), p. 687.
[35] J.M. Luttinger and W. Kohn, Phys. Rev. **97**, 869 (1955).
[36] G. Bastard, *Wave Mechanics Applied to Semiconductor Heterostructures* (Les editions de Physique, Paris, 1988).
[37] J.R. Chelikowsky and M.L. Cohen, *Band Structure and Optical Properties of Semiconductors* (Springer, Berlin, 1987).
[38] R. Enderlein, G.M. Sipahi, L.M.R. Scolfaro, J.R. Leite, and I.F.L. Diaz, Mater. Sci. Eng. B **35**, 396 (1995).
[39] Abraham Moyses Cohen and Gilmar Eugenio Marques, Phys. Rev. B **41**, 10 608 (1990).
[40] R.O. Jones and O. Gunnarson, Rev. Mod. Phys. **61**, 689 (1989).
[41] M. Combescot and P. Nozieres, J. Phys. C **5**, 2369 (1972).
[42] G. Harbeke, O. Madelung, and U. Rössler, in *Physics of Group IV Elements and III-V Compounds*, edited by O. Madelung, Landoldt-Börnstein, New Series, Group III, Vol. 17, Pt. a (Springer-Verlag, Berlin, 1982).
[43] L. Hedin and J. Lundqvist, J. Phys. C **4**, 2064 (1971).
[44] M. Altarelli, U. Ekenberg, and A. Fasolino, Phys. Rev. B **32**, 5138 (1985).
[45] B.W. Kim and A. Majerfeld, J. Appl. Phys. **77**, 4552 (1995).